PHYSICAL REVIEW B VOLUME 34, NUMBER 10 15 NOVEMBER 1986

Classically exact overlayer dynamics: Diffusion of rhodium clusters on Rh(100)

Arthur F. Voter
Theoretical Division (Mail Stop J569), Los Alamos National Laboratory, University of California, P.O. Box 1663, Los Alamos, New Mexico 87545
(Received 30 June 1986)

A new method is presented for describing the classical dynamics (e.g., diffusion, desorption) of adsorbed overlayers of atoms or molecules, starting from arbitrary interatomic potentials. Provided that a certain dynamical criterion is met, the method yields classically exact results, but with many orders of magnitude less computation than direct molecular dynamics. The approach provides, for what we believe to be the first time, a connection between stochastic lattice-gas dynamical methods and the interatomic potential function. As a sample application, the diffusion constants are computed for two-dimensional rhodium clusters of up to 75 atoms on the Rh(100) surface at $T=2000$ K. For clusters larger than $n=15$ atoms, the diffusion constant scales as $n^{-1.76\pm0.06}$, and the dominant mechanism for the diffusion is found to be atoms running along the edges of the cluster blocks.

I. INTRODUCTION

There is currently considerable interest in the dynamics of atoms and molecules adsorbed on surfaces, due to the key role surfaces play in a variety of important processes, and because of advances in experimental methods for characterizing surface events. The current theoretical understanding comes largely from computer "experiments," in which adsorbed atoms or overlayers are dynamically evolved, allowing observation of the physical process of interest. These computer simulations can generally be divided into two classes—molecular-dynamics (MD) simulations, in which the system (adsorbate atoms and substrate atoms) follows a classical trajectory according to the chosen interatomic potential function, and stochastic lattice-gas (LG) simulations, in which a grid of binding sites is occupied with a fractional coverage of atoms and the occupation pattern is evolved by selecting successive atom hops using a Monte Carlo procedure.

The MD approach is usually employed when the desired dynamical property can be extracted from the behavior of a few thousand atoms during a time less than a nanosecond; larger simulations are generally unfeasible. MD simulations have been used, for example, to calculate diffusion constants for single atoms[1–3] and small clusters,[4–6] simulate chemical diffusion of Xe on W(110),[7] observe the "knockout" mechanism for cross-channel diffusion in the Ir/Pt(110) system,[8] and investigate the properties of the crystal-vapor interface.[9] The advantage of the MD approach is that classically exact results are obtained for a given interatomic potential. The interatomic potential can, in principle, be made arbitrarily accurate, allowing critical comparison between MD and experiment. While most MD studies have employed pairwise potentials (e.g., Lennard-Jones 6-12), interatomic potentials that go beyond the pairwise approximation are becoming available.[10,11]

In contrast to MD, the LG approach can be used to calculate dynamical properties for large numbers of adsorbed atoms over long time scales. For example, LG simulations have been used to calculate chemical diffusion constants,[12–16] investigate the relation between tracer and chemical diffusion in overlayers,[17] observe phase transitions,[18,19] domain growth[20,21] and cluster growth,[22,23] and investigate vapor deposition[24] and thermal desorption.[25] However, to treat such systems, the LG method pays some penalties. First, the LG approach can only be applied to systems in which the adsorbate binds in registry with the substrate, since each adsorbed entity (atom or molecule) is assigned to a binding site. Second, the LG method discards all the dynamics occurring on a time scale that is short relative to the time between adatom hops; each adatom simply resides in some binding site, without vibrating. Third, the dynamics do not evolve according to an interatomic potential—the motion and response of the substrate atoms are excluded and the potentials between the adatoms are reduced to a few interaction values which are assumed to be additive. While the first two approximations are intrinsic to the LG approach, the last one can be eliminated—as will be shown here.

We present in this paper a new method for describing overlayer dynamics. *Starting from an arbitrary interatomic potential, this method yields rigorous classical dynamics for large systems over long time scales.* The effect of the motion and dynamical response of the substrate atoms is included in the simulation. As in the LG approach, the method is restricted to systems in which the adsorbed species bind in registry with the substrate. The method can be used to obtain both equilibrium and dynamical properties.

Because the foundation for the method is the dynamical description of a single adatom, Sec. II contains a review of the necessary single-atom results. The new method is then presented in Sec. III. In Sec. IV, the method is used to calculate the diffusion constants of rhodium atom clus-

ters on a Rh(100) surface, and determine the mechanism of cluster migration. Some of the calculations require dynamical evolution for more than ten microseconds.

II. SINGLE-ADATOM DYNAMICS

This section reviews the dynamics of a single atom or molecule migrating on a surface. Transition-state theory (TST) is presented first, followed by the multistate dynamical corrections formalism that, combined with TST, provides a rigorous description of the dynamical behavior of the adsorbed entity (hereafter referred to as the adatom) on a surface.

Begin by defining a lattice of binding sites such that the position of the adatom at any time corresponds to exactly one binding site (or "state"). To apply TST, the motion of the adatom is assumed to consist of independent, randomly oriented hops between adjacent binding sites. The average time the adatom resides in any particular binding site is taken as the inverse of the rate constant for escape from that state. In TST, this escape rate is approximated as the equilibrium flux (assuming a canonical ensemble) of particles exiting through the boundary surface surrounding the state. This boundary, which will be referred to as the TST surface, is a function of the coordinates of the adatom and possibly the substrate atoms. In one dimension, taking the coordinate to be x and defining $x \leqq q$ as state A (i.e., the TST surface is at $x=q$), the TST rate constant for escape from state A is given by[26]

$$k_{A\rightarrow}^{\mathrm{TST}} = \tfrac{1}{2}\langle\, |\dot{x}|\, \delta(x-q)\rangle \,, \tag{1}$$

which for a canonical ensemble simplifies to[27]

$$k_{A\rightarrow}^{\mathrm{TST}} = \frac{1}{2}\left[\frac{2k_BT}{\pi m}\right]^{1/2} \langle \delta(x-q)\rangle_A \,. \tag{2}$$

(Note that the assumption of a canonical ensemble is perfectly appropriate, since the adatom is in constant contact with a nearly infinite heat bath.) Here $\dot{x}$ is the time derivative of x, m is the mass of the particle (the effective mass along the reaction coordinate[28]), $\delta(\ )$ is the Dirac delta function, k_B is the Boltzmann constant, T is the temperature, and $\langle \cdots \rangle_A$ indicates a classical canonical ensemble average over the configuration space of state A. This average can be evaluated exactly using a Monte Carlo procedure;[29] in essence, one simply performs a Metropolis walk[30] over state A, and counts up the fraction of steps that are within a small distance of the TST surface. Computing this average in many dimensions is straightforward.[29]

The TST approximation does not given the true dynamical rate constant because each crossing of the TST surface does not necessarily correspond to a reactive state-change event. During a reactive conversion from state A to state B, the system may cross the TST surface a number of times before thermalizing in state B. Alternatively, an even number of crossings may take place, leaving the system in state A, corresponding to no reaction. In a two-state system, these "correlated dynamical events" cause k^{TST} to be an upper bound on the true rate constant, since each reactive state-change event consists of at least one TST surface crossing. In a many-state system the situation is more complicated.

For two-state systems, methods for performing dynamical corrections to TST are well known,[31,32] and an elegant reactive flux formalism has been developed by Chandler.[32] Define τ_{corr} as the time required for the correlated dynamical events (spurious recrossings) to cease after an initial crossing, and define τ_{rxn} as the average time between reactive state-change events (i.e., the inverse of the true rate constant). For systems that satisfy

$$\tau_{\mathrm{corr}} \ll \tau_{rxn} \,, \tag{3}$$

he showed that the dynamically exact rate constant can be expressed as

$$k_{A\rightarrow B} = k_{A\rightarrow}^{\mathrm{TST}} f_d \,, \tag{4}$$

where the dynamical correction factor, f_d $(0<f_d\leqq 1)$, is evaluated from the behavior of classical trajectories initiated at the TST surface and evolved for a time τ_{corr}. These trajectories account for the ultimate fate of each surface crossing counted by TST, filtering out those that do not correspond to a true reactive event.

To treat the case of an adatom on a surface, one must also account for the possibility that the energized adatom will make a correlated multiple hop, thermalizing in a nonadjacent binding site. We have recently presented an extension of the dynamical corrections theory for treating many-state systems such as this.[33] When Eq. (3) holds, the rate constant between *any* two states (i and j) of the system, whether or not they are connected in configuration space, is given by

$$k_{i\rightarrow j} = k_{i\rightarrow}^{\mathrm{TST}} f_d(i\rightarrow j) \,, \tag{5}$$

where k_i^{TST} is the total TST escape rate from state i (the TST flux through all TST surfaces bounding state i). The state-dependent dynamical correction factor $f_d(i\rightarrow j)$ is computed from trajectories initiated at the TST surface surrounding state i,

$$f_d(i\rightarrow j) = \frac{2}{N}\sum_{I=1}^{N} \gamma(I)\Theta_j(I) \,. \tag{6}$$

Here N is the number of trajectories, the phase factor $\gamma(I)$ is $1(-1)$ is trajectory I is initially exiting (entering) state i, and $\Theta_j(I)=1$ if trajectory I is in state j at time τ_{corr}, and zero otherwise. [Note that in Ref. 33, the factor of N^{-1} was accidently omitted from Eq. (4.6).] If all trajectories immediately thermalize in the states towards which they are initially traveling, then $k_{i\rightarrow j}=k_{i\rightarrow}^{\mathrm{TST}}$ for all states j adjacent to i, and $k_{i\rightarrow j}=0$ for nonadjacent i and j. Trajectories that recross the initial TST surface act to reduce the correction factor for adjacent states (as in the two-state case), and trajectories that make multiple hops, thermalizing in a nonadjacent state, give rise to a nonzero correction factor for that state.

To illustrate the use of TST plus dynamical corrections, consider the diffusion of a rhodium atom on a Rh(111) surface, modeled using a Lennard-Jones 6-12 potential. (The calculation is discussed in detail in Ref. 33.) The TST surface is defined by connecting four substrate atoms with vertical planes, as shown in Fig. 1. The planes are

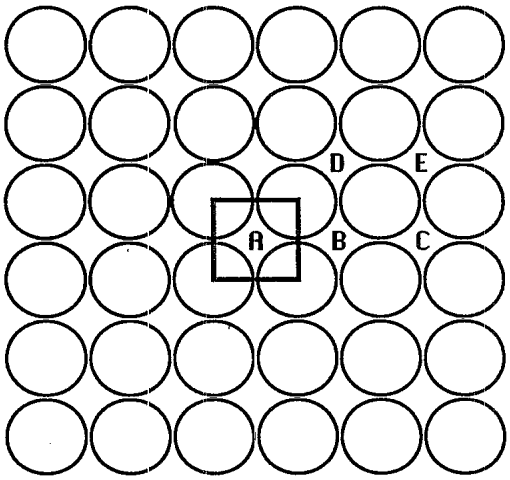

FIG. 1. Rh(100) substrate. The TST planes surrounding binding site A are shown (the adatom is omitted). Possible nearby final states (B,C,D,E) are also indicated.

fixed at the equilibrium positions of the substrate atoms so that the TST surface depends only on the x and y coordinates of the adatom. Once a temperature is specified, the rigorous TST rate constants are computed using a Metropolis Monte Carlo procedure.[29,34] Starting conditions for a number of classical trajectories are then chosen by sampling from a Metropolis walk restricted to this same TST surface, half of them initially entering state A, and half initially exiting. (Due to the symmetry of this particular system, all necessary information is contained in trajectories initiated in one direction from one of the four planes.) These trajectories are integrated until all the state-to-state transitions have ceased (this defines τ_{corr}), and the rate constants are computed using Eqs. (5) and (6). In both the TST and the dynamical corrections calculations, the first layer of substrate atoms are allowed to move, while deeper layers are fixed.

Table I displays the results of calculations up to a temperature of 1000 K; above this temperature the system begins to violate the requirement of Eq. (3). The diffusion constants are computed from

$$D=\tfrac{1}{4}\sum_{j\ (\neq i)} k_{i\to j} l_{ij}^2 , \tag{7}$$

where l_{ij} is the distance between binding sites i and j. As expected, the correlated dynamical effects are seen to increase with temperature. Even at the highest temperature, however, the magnitude of the corrections is small. This is true in all the Lennard-Jones systems we have investigated.

Also included in Table I are rate constants computed using a simple approximate form of TST (STST), in which

$$k^{\text{STST}}=n_p \nu_0 \exp[-(E_{\text{saddle}}-E_{\text{min}})/k_B T] , \tag{8}$$

where n_p is the number of possible exit directions ($n_p=4$ for a square lattice), ν_0 is the harmonic frequency, and E_{saddle} and E_{min} are the energies at the transition state between two binding sites and at the minimum, respectively. These energies are found by performing a Newton-Raphson search for stationary points in the hyperspace defined by the Cartesian coordinates of all the moving atoms. At each of these two geometries, the 3×3 matrix of second derivatives for motion of just the adatom is computed and diagonalized, and the frequency associated with each eigenvalue b_i is calculated from

$$\nu_i=\frac{1}{2\pi}\left[\frac{b_i}{m}\right]^{1/2} , \tag{9}$$

where m is the adatom mass. The pre-exponential factor ν_0 is computed from

$$\nu_0=\frac{\nu_{1m}\nu_{2m}\nu_{3m}}{\nu_{2s}\nu_{3s}} , \tag{10}$$

where ν_{1m}, ν_{2m}, and ν_{3m} are the frequencies at the minimum, and ν_{2s} and ν_{3s} are the two nonimaginary frequencies at the saddle point. Note that the STST rate constants give a reasonable approximation to the exact TST rate constants, and also to the dynamically exact rate constants.

III. OVERLAYER DYNAMICS

In this section we develop a method for describing the classical dynamical evolution of an arbitrary pattern of interacting adsorbed species. Though the method yields dynamical information only for time scales that are long relative to the time between individual atom hops, all the effects of the dynamics occuring on a short time scale are rigorously accounted for. The method is restricted to systems in which the adsorbed atoms or molecules bind in registry with the surface. The binding sites may be of any type (e.g., atop, bridge, or hollow), but they must form a

TABLE I. Rate constants and dynamical correction factors for Rh/Rh(100). The k^{TST} values were obtained from a Monte Carlo evaluation of Eq. (2) [with statistical uncertainty of $\pm10\%$, and the k^{STST} values were computed using Eq. (8)]. The dynamical corrections factors, $f_d(i\to j)$, were computed from the results of 100 to 200 classical trajectories at each temperature, using Eq. (6). The state designations (A,B,C,D) are defined in Fig. 1. Note that $f_d(A\to B)=0.25$ corresponds to TST.

T	$k_{A\to}^{\text{TST}}$ (s^{-1})	$k_{A\to}^{\text{STST}}$ (s^{-1})	$f_d(A\to B)$	$f_d(A\to C)$	$f_d(A\to D)$	$f_d(A\to E)$	D/D^{TST}
200	3.3×10^{-13}	2.4×10^{-13}	0.25	0.0	0.0	0.0	1.000
300	1.4×10^{-4}	1.1×10^{-4}	0.25	0.0	0.0	0.0	1.000
500	1.3×10^{3}	9.1×10^{2}	0.2467	0.0017	0.0	0.0	1.013
1000	2.1×10^{8}	1.4×10^{8}	0.2088	0.0100	0.0050	0.0062	1.060

regular lattice. For simplicity, the discussion will be based on a square lattice, though any type of lattice can be treated.

Consider a submonolayer distribution of adatoms over the lattice of binding sites, and focus on one adatom (the "primary" adatom) and its particular environment. The method is based on the following three premises, which are true if the above restrictions hold.

(i) The classical dynamics of the adatom and its environment can be rigorously described by combining TST with multistate dynamical corrections, provided there is a separation of time scales as defined by Eq. (3).

(ii) The rate constant for the escape of the adatom from its binding site, and the probability distribution of possible final states of the system after the transition, will depend on the local environment of the adatom. Note that the state of the system depends on the position of every adatom, not simply the primary adatom; a hop by the primary adatom may induce correlated hops in nearby atoms—these are taken into account by the dynamical corrections trajectories.

(iii) This rate constant and final-state distribution will *not* depend significantly on the environment beyond a certain distance from the adatom and, conversely, adatoms beyond a certain distance will essentially never be affected by a primary adatom event.

The consequence of these premises is that the rate constants for all possible final states resulting from an adatom hop can be rigorously evaluated if the local environment is known. The essence of the method is to precalculate these rate constants for all possible initial states of the local environment and store this dynamical information in a catalog, indexed by the initial state. This catalog is then used to propagate any desired overlayer pattern.

As a working example, consider an adatom on a square lattice and the adjacent empty binding site that it will occupy if it makes a simple hop to the right, as shown in Fig. 2. Defining the local environment to be the ten binding sites immediately surrounding these two sites, the number of possible states of the environment is 2^{10}, corresponding to each of the ten sites being empty or occupied (some of these states will be equivalent by symmetry). For each of these 1024 states, rate constants are calculated at a chosen temperature for all possible final states (arising from an initial adatom hop to the right) using TST and dynamical corrections trajectories as described in Sec. II. In these calculations, the complete interatomic potential is employed, and the motion and response of the substrate atoms are included. The dynamical corrections trajectories allow for the possibility that secondary adatoms make hops in response to the primary adatom hop. The catalog thus consists of 1024 entries, where each entry is composed of an escape rate $k_{\rm esc}$ (which is the sum of the rate constants for that initial state) and a list of probabilities for transitions to various possible final states.

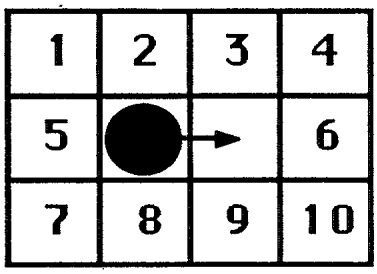

FIG. 2. Ten-atom local environment for an adatom hopping to the right on a square lattice. Each of the ten binding sites may be empty or occupied, leading to 2^{10} possible environments.

Armed with this catalog, any overlayer pattern of $N_{\rm atom}$ adatoms can be dynamically evolved at this temperature using the following procedure.

(i) Use the catalog to look up the appropriate value of $k_{\rm esc}$ for each of the $4N_{\rm atom}$ possible hops (each atom has four possible hop directions). For hops that are blocked by an adatom in the adjacent binding site, $k_{\rm esc}=0$.

(ii) Increment the clock by

$$\Delta t_{\rm hop}=\left[\sum_{i=1}^{4N_{\rm atom}} k_{\rm esc}(i)\right]^{-1}, \tag{11}$$

which is the time, on average, before *some* atom in the overlayer makes a hop.

(iii) Randomly select one of the $4N_{\rm atom}$ possible hops, weighting the probability of selection of each hop by $k_{\rm esc}$. Randomly select a final state, using the probabilities in the appropriate catalog entry. Modify the position of the chosen adatom and its local environment to put it into this final state.

(iv) Go to (i).

Because this procedure utilizes a catalog of rate constants that are classically exact (for the chosen interatomic potential), the resulting dynamical evolution is correct for long time scales. The only approximation lies in truncating the local environment at ten atoms; this approximation can be eliminated by increasing the size of the local environment until the catalog of rate constants is unaffected by a further increase. In practice, of course, the environment can be chosen to give errors smaller than a desired threshold. All dynamical properties that can be calculated with standard lattice-gas methods, such as tracer and chemical diffusion constants, autocorrelation functions of adsorbate density fluctuations, island nucleation rates, etc., can also be computed using the present method. The method is independent of the interatomic potential, as long as the adsorbate binds in registry and Eq. (3) is satisfied. This approach, for the first time, provides a connection between stochastic lattice-gas techniques and the interatomic potential.

Treating desorption with this method is also straightforward. The rate constant catalog is augmented to include rate constants for desorption of an adatom. The TST desorption rate constant for a given environment is computed from the flux through a plane, parallel to the surface, that caps the top of the binding site. Dynmical corrections are computed by initiating trajectories from this plane, and following them for a time $\tau_{\rm corr}$. (The dynamical correction factor for simple desorption of the primary adatom is essentially the thermal sticking coefficient.)

The method can also be applied to cases in which mul-

tiple crystal layers are simultaneously exposed, e.g., for treating the diffusion of adatoms over a stepped surface, or in modeling crystal growth or surface roughening. In principle, the catalog indexing is simply extended to include all neighboring atoms that can influence the primary atom. In practice, the local environment must be expanded judiciously, since the catalog size grows exponentially with the size of the local environment.

IV. DIFFUSION OF RHODIUM CLUSTERS

Clustering of adsorbed atoms and molecules is a widespread phenomenon, important in thin-film[35] and crystal[36,37] growth, and evident in a variety of surface science experiments. Though clusters were once thought to be completely immobile, it is now recognized that they can diffuse on the surface,[4,5,38–44] contributing to cluster growth and mass transport. The motions of small clusters ($n=2$ to $n=10$) have been investigated experimentally using field ion microscopy,[41,43,44] and theoretically using molecular dynamics,[4,6] and other models,[45,46] and diffusion constants have been obtained theoretically for clusters as large as $n=6$.[4] Dynamics of larger clusters have been studied[47] in one dimension using the Frank and van der Merwe model,[48] but almost nothing is known about the dynamics of larger two-dimensional clusters. As a demonstration of the method described in this paper and to provide some insight into the motion of large clusters, we examine the diffusion of two-dimensional rhodium clusters on the Rh(100) surface at $T=2000$ K.

A. Calculational details

The rhodium was modeled using a Lennard-Jones 6-12 pair potential with a fifth-order spline to make the pair energy go smoothly to zero at the cutoff distance. Thus, the total energy is given by

$$V=\frac{1}{2}\sum_{\substack{i,j\\ i\neq j}}\phi(r_{ij}) , \tag{12}$$

with

$$\phi(r_{ij})=\begin{cases} 4\epsilon[(\sigma/r_{ij})^{12}-(\sigma/r_{ij})^{6}], & 0<r_{ij}<r_1 \\ \displaystyle\sum_{k=0}^{5} c_k (r_{ij})^k, & r_1\le r_{ij}\le r_2 \\ 0, & r_2<r_{ij} , \end{cases} \tag{13}$$

where r_{ij} is the distance between atoms i and j, and the coefficients $\{c_k\}$ are determined by the requirement that $\phi(r_{ij})$ be continuous and have continuous first and second derivatives at r_1 and r_2. After choosing $r_2=2.5\sigma$, r_1 was determined by minimizing the maximum absolute deviation between the spline and the Lennard-Jones potential over the range r_1 to r_2, leading to $r_1=1.5\sigma$. The values for σ and ϵ were those parametrized from bulk thermodynamic data by Doll and McDowell[1] ($\sigma/k_B=7830$ K, $\epsilon=2.47$ Å). Note that the results presented here are not directly comparable with previous studies using this rhodium potential,[1,29,33] nor with the results presented in Table I, because those studies used a cutoff with an energy shift that changed the well depth.

While the quantities (e.g., energies and diffusion constants) quoted here will be appropriate for the Rh/Rh(100) system, they can be converted to standard Lennard-Jones reduced units using the usual corresponding-states relations for energy, distance, temperature, and time,

$$\begin{aligned} E^*&=E/\epsilon , \\ r^*&=r/\sigma , \\ T^*&=k_B T/\epsilon , \\ t^*&=t(\epsilon/m\sigma^2)^{1/2} . \end{aligned} \tag{14}$$

Thus, the present study corresponds to a reduced temperature of $T^*=0.2554$, and the energies (kcal/mol), times (sec) and diffusion constants (cm^2/sec) reported here can be transformed to reduced units using the conversion factors 509.0 sec/cm^2, 3.220×10^{12} sec^{-1}, and 0.06427 mol/kcal, respectively.

The rhodium substrate was modeled using a four-layer block of atoms with 42 atoms (7×6) per layer, as shown in Fig. 3. Periodic boundary conditions were employed in the two directions parallel to the surface. On top of this block were placed the adatom and between zero and ten neighboring adatoms. The adatoms and all the atoms in the top layer of substrate were allowed to move in the calculations, while the atoms in the lower layers were frozen with a nearest-neighbor distance of $2^{1/6}\sigma$ (lattice constant equals 3.921 Å). The layer size was chosen so that the distance between any adatom and the periodic image of any other adatom was greater than the 2.5σ cutoff distance, and the number of layers was chosen so that no moving atom was within the cutoff distance of the omitted fifth layer.

The adatom environment was defined by the ten binding sites shown in Fig. 3, matching the example discussed

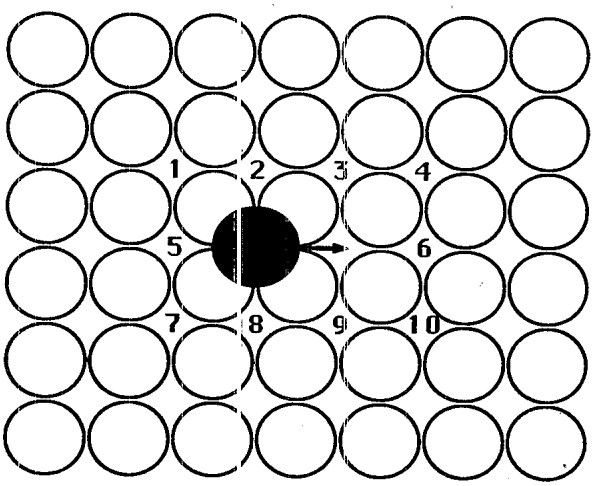

FIG. 3. Top layer of the substrate pad used for the Rh_n/Rh(100) cluster study. The ten binding sites making up the local environment are indicated. All atoms shown are allowed to move in computing the 1024 rate constants.

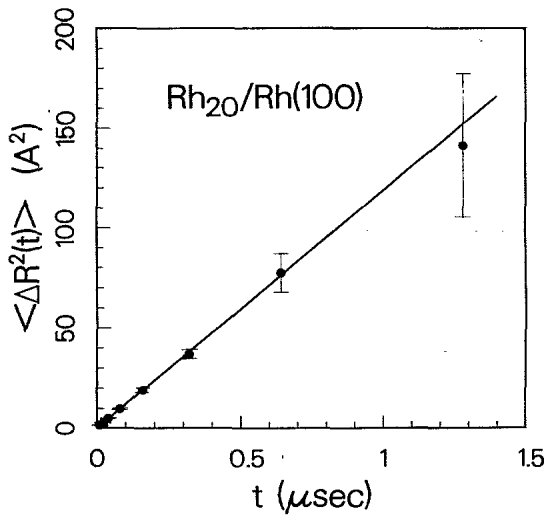

FIG. 4. Mean-squared displacement for a 20-atom Rh cluster at $T=2000$ K.

in Sec. III. Because of the preliminary nature of this study, and because the dynamical corrections have been shown to be small in this type of system, the 1024 rate constants in the catalog were computed using the STST method described at the end of Sec. II. To reduce the probability of error, the catalog generation process was automated. The program looped over the 1024 possible values of the environment index, performing the following procedure for each value: (1) Determine whether the current environment is related by symmetry to one previously calculated—if so, skip to step (7). (2) Position the primary adatom and the n secondary adatoms ($0 \leqq n \leqq 10$) at reasonable starting positions in their respective binding sites. (These positions, and the positions for all the substrate atoms, are taken from a previously performed energy minimization involving the substrate and all 11 adatoms.) (3) Perform a Newton-Raphson-style search in the $3(1+n+42)$-dimensional space of Cartesian coordinates to find the geometry $R_{\min}$ and energy $E_{\min}$. (It was found that using only the diagonal curvature matrix elements (e.g., d^2E/dy_1^2) yielded the desired energy-minimized geometry in less computer time than using the full $[3(1+n+42)]^2$-element curvature matrix.) (4) Position the adatom at a reasonable starting guess for the saddle-point geometry (without moving the other atoms). (5) Perform a search for the saddle-point geometry R_{saddle} and energy E_{saddle}, using the diagonal curvatures plus the three unique off-diagonal curvatures involving only the primary adatom. If this fails to converge to a saddle point (defined by a zero gradient and one negative eigenvalue of the 3×3 curvature matrix), perform the search again using the full curvature matrix, checking that the full curvature matrix at R_{saddle} has exactly one negative eigenvalue. (6) Using the 3×3 primary adatom curvature matrices at R_{saddle} and $R_{\min}$, compute the frequencies ν_{1m}, ν_{2m}, ν_{3m}, ν_{2s}, and ν_{3s} from Eq. (9) and fold these into the pre-exponential factor ν_0 using Eq. (10). Compute the activation energy

$$E_{\text{act}}=E_{\text{saddle}}-E_{\min} . \tag{15}$$

(7) Store E_{act} and ν_0 in the catalog under the appropriate environment index.

The STST approximation, in addition to allowing economical computation of the rate constant catalog, provides a catalog that can be used at any temperature, since each rate constant is computed from

$$k=\nu_0 \exp(-E_{\text{act}}/k_B T) . \tag{16}$$

A temperature of 2000 K was chosen for the present study. While this is above the temperature where the separation of time scales strictly holds, it is sufficiently low for this preliminary study. At 2000 K, τ_{rxn} is approximately ten times τ_{corr} for a single Rh atom on the

TABLE II. Cluster diffusion results for Rh_n/Rh(100). Δt is the time interval between recorded configurations.

n	Δt (sec)	Configurations recorded	Total hops	Hops rejected	D_n (cm^2/sec)
1					7.4×10^{-6}
2	5×10^{-9}	2000	4.7×10^{5}	34 594	$(2.1\pm0.1)\times10^{-6}$
3	10^{-8}	2000	3.3×10^{6}	39 233	$(5.8\pm0.3)\times10^{-7}$
4	10^{-8}	2000	1.2×10^{6}	14 445	$(1.3\pm0.3)\times10^{-7}$
5	10^{-8}	2000	2.3×10^{6}	13 000	$(1.1\pm0.1)\times10^{-7}$
6	10^{-8}	2000	1.4×10^{6}	8700	$(5.0\pm0.4)\times10^{-8}$
7	10^{-8}	2000	2.0×10^{6}	8600	$(4.4\pm0.3)\times10^{-8}$
8	10^{-8}	2000			$(2.1\pm0.2)\times10^{-8}$
9	10^{-8}	2000			$(2.0\pm0.1)\times10^{-8}$
10	10^{-8}	2000	1.5×10^{6}	5782	$(1.5\pm0.1)\times10^{-8}$
11	10^{-8}	2000			$(1.02\pm0.05)\times10^{-8}$
12	10^{-8}	2000			$(9.2\pm0.3)\times10^{-9}$
15	2×10^{-8}	2000			$(5.35\pm0.15)\times10^{-9}$
20	2×10^{-8}	2000	1.6×10^{6}	3547	$(3.0\pm0.17)\times10^{-9}$
30	10^{-8}	2000			$(1.6\pm0.1)\times10^{-9}$
50	4×10^{-8}	1877	1.9×10^{6}	3240	$(6.5\pm0.5)\times10^{-10}$
75	2×10^{-8}	1680			$(3.0\pm0.5)\times10^{-10}$

Rh(100) surface. To obtain Arrhenius activation energies, a few runs were performed at temperatures above or below 2000 K.

Clusters up to size $n=75$ were examined, using an independent dynamical simulation for each cluster size. Each simulation was performed on a square grid using periodic boundary conditions, with the grid chosen large enough that the cluster did not interact with its periodic image. The following describes the procedure for calculating the diffusion constant for a cluster of size n.

The initial cluster configuration was generated by successively placing atoms at random positions on the grid, rejecting any placement that was not within nearest-neighbor or next-nearest-neighbor distance of an existing atom, until n atoms were successfully placed. The connectivity of the initial cluster was thus guaranteed. The cluster configuration was then evolved in time, using the procedure of Sec. III. (Since the number of atoms in the simulation was relatively small, the rate constants were looked up for all the atoms after each hop. If thousands of atoms were involved, a faster approach would be to refresh the rate constants for only those atoms whose environments had changed.) The dynamics evolved with the restriction that if a chosen atom hop broke the cluster connectivity, the clock was incremented, but that hop was *not* performed. This nonphysical restriction was imposed so that the diffusion constant could be computed for a well-defined cluster, rather than fragments of a cluster. [Note that allowing "connected" atoms to be as far apart as fourth-nearest neighbors ($5^{1/2}l$) resulted in *no* statistically significant change in the $n=10$ diffusion constant.] During the simulation, after an initial equilibration period of 1000 steps, cluster configurations were saved at uniform time intervals (Δt), and the run was continued until 2000 of these configurations had been saved. The diffusion constant was then calculated from the time evolution of the mean-squared displacement of the cluster center of mass,

$$D_n = \lim_{t\to\infty}\left[\frac{1}{4}\frac{d}{dt}\langle \Delta R^2_{\rm cm}(t)\rangle\right], \tag{17}$$

as shown in Fig. 4. Error estimates were obtained by subdividing the trajectory into pieces that were analyzed independently.

To obtain valid statistics, the recording time interval Δt should be long enough that many hops occur between successive recordings. Since the time between hops ($\Delta t_{\rm hop}$) depends on the configuration, the number of hops per recording varies. Table II shows that the average number of hops per recording ranged from 200 to 1000, depending on cluster size, and it was never the case that two successive recorded configurations occurred without an intervening hop.

All calculations were performed on a Digital Equipment Corporation VAX11/780 minicomputer with floating-point accelerator. Generation of the catalog took about 20 h of CPU (Central processing unit) time. The CPU time required for the dynamical simulations was proportional to the total number of atom hops, and scaled as the number of atoms for large clusters (this dependence would be reduced if rate constants were updated only for the necessary atoms). The 20-atom case took 4.5 CPU hours.

B. Results and discussions

To gain a qualitative understanding of the overlayer dynamics in this system, it is instructive to examine the rate constants as a function of adatom environment. Figure 5 shows some representative activation energies from the rate catalog. The barrier to diffusion for a single adatom [Fig. 5(a)] is 25.3 kcal/mol, while the barrier for an atom to make a jump away from a nearest-neighbor atom [Fig. 5(b)] is 38.7 kcal/mol. The overlayer interactions are thus attractive, as expected, and the atoms tend to cluster. The other activation barriers displayed support this conclusion. Figure 5(f) shows that the barrier for an atom moving along the edge of a block of atoms is only 18.5 kcal/mol, much less than the barrier for an atom to step out from the side [55.3 kcal/mol, Fig. 5(d)] or corner

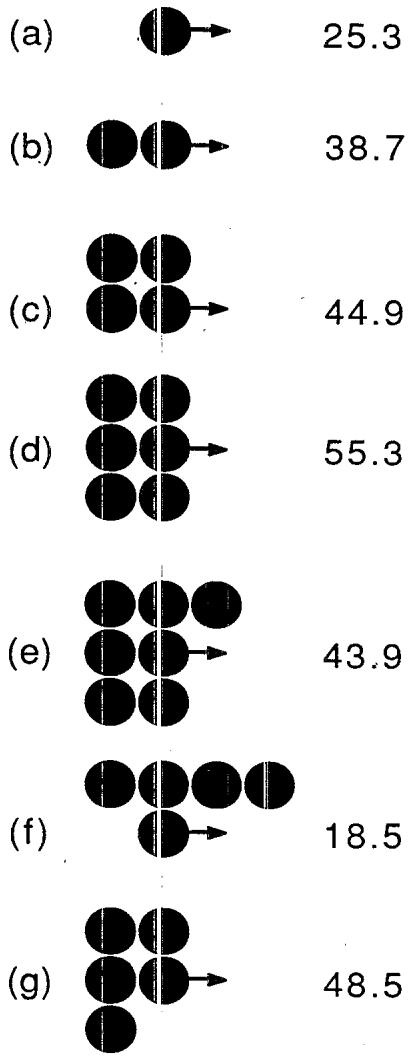

FIG. 5. Some representative activation barriers (kcal/mol) from the rate catalog. All the catalog values for ν_0 [Eq. (16)] are between 4.8×10^{12} and 1.2×10^{13} sec^{-1}.

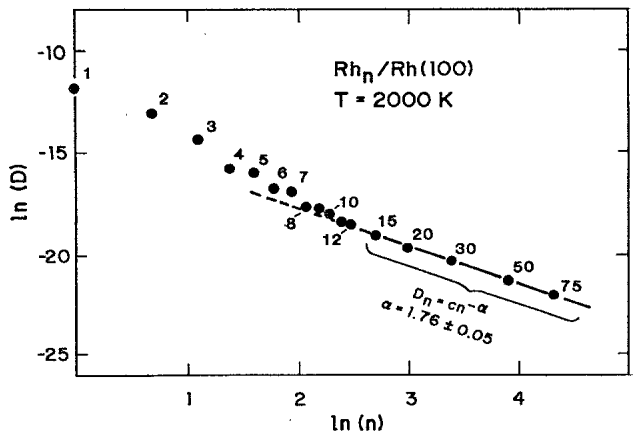

FIG. 6. Diffusion constants for Rh_n clusters on Rh(100). Units for D_n are $cm^2 sec^{-1}$.

[44.9 kcal/mol, Fig. 5(c)] of a block of atoms. At low enough temperatures that clusters tend to form tightly packed blocks, the vast majority of the atom jumps are single atoms running along the edges of the blocks. Even at 2000 K, the clusters tend to pack into blocks, and edge running is common.

The cluster diffusion results at 2000 K are displayed in Table II and Fig. 6. The diffusion constant is seen to decrease monotonically with increasing cluster size. Small clusters that can form stable blocks ($n=4,6,8$) diffuse more slowly than expected from the diffusion rates of the nearby cluster sizes. This is because a long time is required to break out of a perfect block structure. At lower temperatures, this effect is so dominant that D_n no longer decreases monotonically with n. This can be seen in the Arrhenius plot in Fig. 7; the Arrhenius activation barriers are 33.4±0.4 kcal/mol, 45.3±0.4 kcal/mol, and 35.2±0.3 for $n=5$, 6, and 7, respectively. This higher barrier for $n=6$ is consistent with an atom breaking out of the

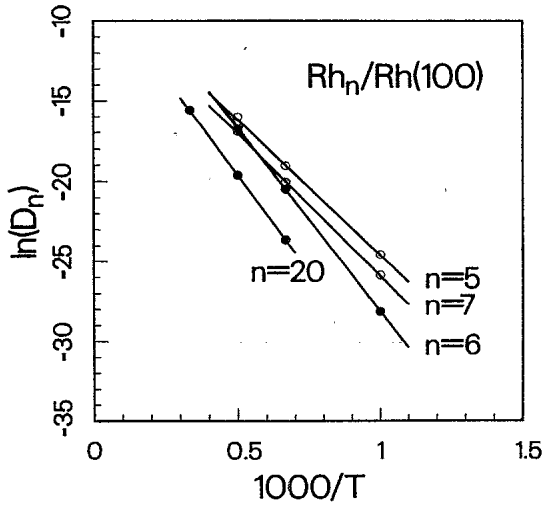

FIG. 7. Arrhenius plot for diffusion of Rh_n clusters on Rh(100).

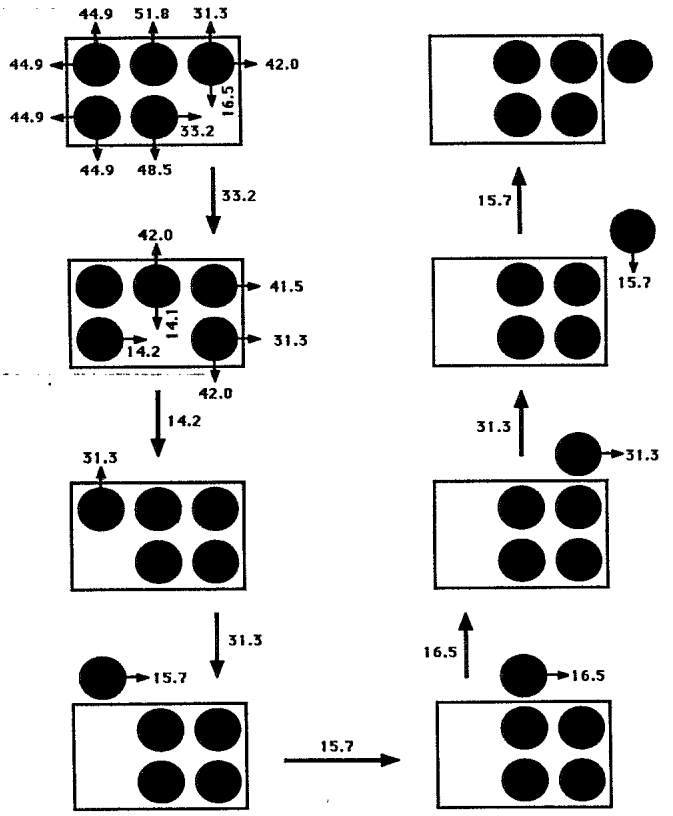

FIG. 8. Diffusion pathway for $n=5$ cluster, effecting replication of original cluster shape, displaced one lattice spacing to the right, in eight moves. The numbers are activation barriers in kcal/mol. The maximum barrier in the eight-move pathway is 33.2 kcal/mol.

corner of a perfect block. Figure 8 shows a possible diffusion pathway for an $n=5$ cluster. The highest barrier in the eight-step mechanism is 33.2 kcal/mol, in excellent agreement with the Arrhenius value. The $n=7$ cluster can also be propagated with a maximum barrier of 33.2 kcal/mol, though the actual mechanism in this temperature range must be more complex, since the observed Arrhenius barrier is 2 kcal/mol higher. (The barrier has a slight temperature dependence, increasing with temperature.)

For clusters larger than ~10 atoms, the diffusion constant shows an interesting power-law dependence,

$$D_n = cn^{-1.76\pm0.06}, \tag{18}$$

with $c = 6.23\times10^{-7}\times[(1.18)^{\pm1}]$. In modeling surface processes at a more macroscopic level, where the motions of entities such as clusters are evolved instead of individual atoms, an analytical expression is required for the dynamical properties of these entities. Equation (18) provides such an expression, and makes a rigorous connection with a particular interatomic potential.

Also of interest is the particular form of Eq. (18), as it relates to the diffusion mechanism. Simple models for the mechanism of cluster diffusion predict a weaker dependence on the cluster size.[49] While we cannot presently ex-

plain the particular n dependence in Eq. (18), it does suggest that a common mechanism exists for the diffusion of clusters larger than approximately 15 atoms. Evidence is presented here that the dominant mechanism for diffusion is edge running, as suggested previously.[5]

Figure 9 shows the shape and relative position of a 50-atom cluster at 2 μsec intervals during the diffusion process. As stated above, the cluster tends to be fairly tightly packed; some configurations correspond to almost perfect rectangular blocks. A single atom running along the edge of one of these blocks has a very low activation barrier [18.5 kcal/mol—see Fig. 5(f)]. Thus, once an atom has been "activated" and is free on an edge, it is extremely mobile. The Arrhenius activation energy for diffusion of these large clusters is 48 ± 1 kcal/mol, as shown in Fig. 7 for $n=20$. This corresponds very well with the barrier of 48.5 kcal/mol for an atom to climb up onto an edge from a kink site, as shown in Fig. 10. Once the atom is free on the edge, it can go around a corner with a maximum barrier of 31.3 kcal/mol (see Fig. 8), and thus can travel around the whole block. Note that while atoms can break away from kink sites with a barrier of 31.9 kcal/mol, the overall cluster motion will stagnate unless atoms climb up onto a fresh edge, which requires 48.5 kcal/mol. Figure 11 shows the time evolution of a 50-atom cluster, with the atoms initially on the right edge of the cluster marked so that their movements can be traced (there are approximately 100 atomic hops between displayed configurations). The evolution of the tagged atoms is consistent with the mechanism proposed here. The results of the edge running are fairly obvious. Later (at longer times than are shown), after new surfaces have been formed and subsequently covered by the random process, the tagged atoms are dispersed randomly throughout the cluster.

In a preliminary report on this work,[50] it was speculated that the rate limiting step for diffusion was the forma-

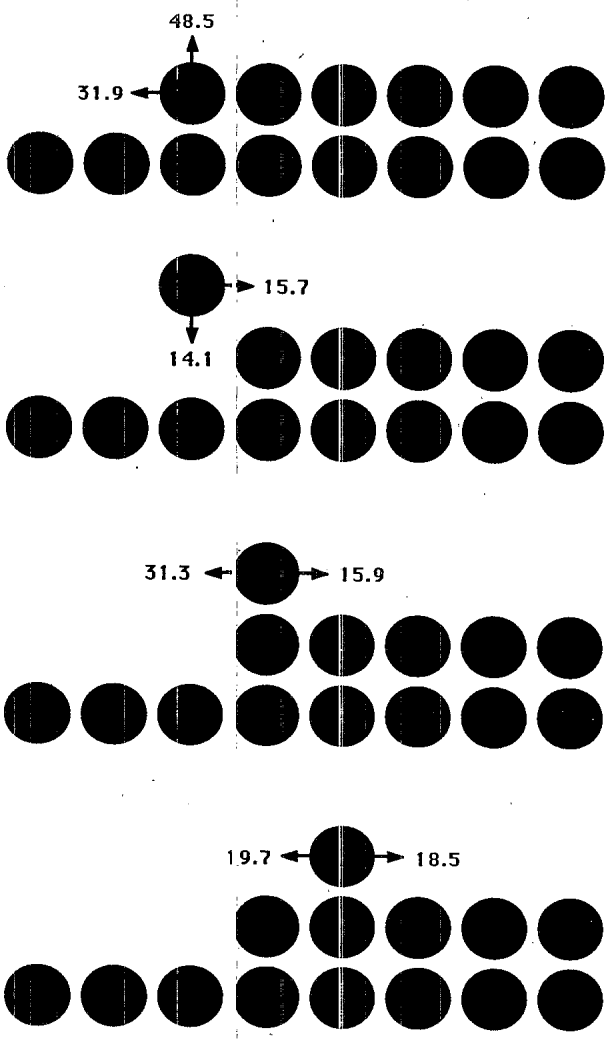

FIG. 10. Mechanism for an atom to climb onto a fresh edge from a kink site. The maximum barrier is 48.5 kcal/mol.

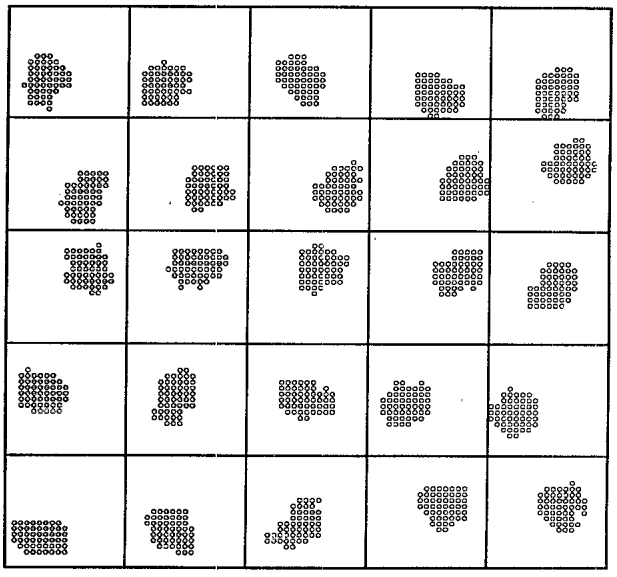

FIG. 9. Time evolution of the shape and relative position of a 50-atom cluster at $T=2000$ K. Displayed configurations are 2 μsec apart, ordered left to right, and then down.

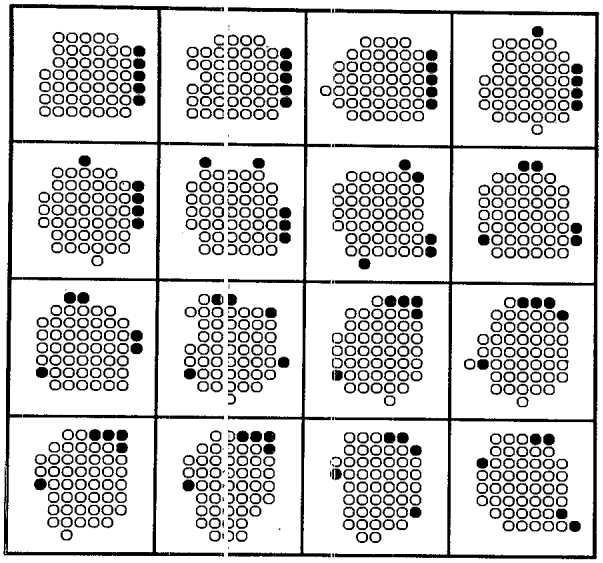

FIG. 11. Time evolution of 50-atom cluster at $T=2000$ K, with some atoms marked to display the edge-running mechanism of diffusion. Displayed configurations are 4×10^9 sec apart (approximately 100 hops), ordered left to right, and then down.

tion of a two-atom fingerlike protrusion on the edge of a block. This was based on the observation that the fractional occurrence of such protrusions scaled with the cluster size in the same way as the diffusion constant [Eq. (18)], the Arrhenius activation barrier was consistent with the formation of this structure, and running the cluster dynamics with this formation artifically excluded led to an 80% decrease in the diffusion constant for a 15-atom cluster. However, it was later observed that the diffusion constants of larger clusters were not affected by this restriction, so this mechanism no longer appears reasonable.

Another way that a cluster can move is by passing atom vacancies through the cluster. For a one-dimensional cluster, this is the only possible mechanism for diffusion. However, for an attractive system in two (or more) dimensions, the formation of a vacancy requires more energy than the formation of a free edge-running atom; the difference is roughly three nearest-neighbor interactions. Thus, the equilibrium concentration of vacancies is expected to be much lower than edge runners. If vacancy motion were dominant, the tagged atoms in Fig. 11 would show much less movement, since passage of a vacancy leaves the atom positions relatively unchanged. Note that if a vacancy is formed, it is fairly mobile ($E_A = 27.0$ kcal/mol); it is thus possible that at very high temperatures, or for very large clusters (due to entropy effects), vacancy motion might contribute significantly to the cluster diffusion.

V. CONCLUSIONS

The method presented here for evolving the classical dynamics of adsorbed overlayers should prove useful in a variety of applications. While stochastic lattice-gas simulations are not new, this method provides, for the first time, a connection between the dynamics and the interatomic potential. If the separation of time scales required by Eq. (3) is met and the local environment is large enough, the resulting dynamics are classically exact. Relaxing either of these restrictions leads to a well-defined level of approximation. The method can be applied to both diffusion and desorption events and can in principle be extended to treat arbitrarily rough surfaces. If reaction probabilities are included in the catalog, surface catalytic reactions can be modeled.

Modeling the diffusion of rhodium clusters on Rh(100) at $T = 2000$ K revealed a number of interesting features. The diffusion constants decrease monotonically with cluster size. For clusters smaller than about ten atoms, clusters that can form stable blocks tend to diffuse more slowly than predicted by interpolation, and at lower temperatures this effect is pronounced enough to lead to nonmonotonic behavior. Diffusion constants of clusters with 15 to 75 atoms (the largest studied) are found to obey a power-law dependence on cluster size [Eq. (18)], and display an Arrhenius activation barrier of 48 ± 1 kcal/mol. The cluster motion arises from single atoms running along the block edges.

ACKNOWLEDGMENTS

The author is grateful to J. D. Doll for many helpful discussions.

[1]J. D. Doll and H. K. McDowell, J. Chem. Phys. **77**, 479 (1982); H. K. McDowell and J. D. Doll, *ibid.* **78**, 3219 (1983).
[2]H. K. McDowell and J. D. Doll, Surf. Sci. **121**, L537 (1982); J. D. Doll and H. K. McDowell, *ibid.* **123**, 99 (1982).
[3]M. R. Mruzik and G. M. Pound, J. Phys. F **11**, 1403 (1981).
[4]J. C. Tully, G. H. Gilmer, and M. Shugard, J. Chem. Phys. **71**, 1630 (1979).
[5]S. H. Garofalini, T. Halichioglu, and G. M. Pound, J. Vac. Sci. Technol. **19**, 717 (1981).
[6]S. H. Garofalini, T. Halichioglu, and G. M. Pound, Surf. Sci. **114**, 161 (1982); S. M. Levine and S. H. Garafalini, *ibid.* **163**, 59 (1985).
[7]S. M. Valone and J. D. Doll, Surf. Sci. **139**, 478 (1984).
[8]S. H. Garofalini and T. Halichioglu, Surf. Sci. **104**, 199 (1981); **112**, L775 (1981).
[9]J. Q. Broughton and G. H. Gilmer, J. Chem. Phys. **79**, 5095 (1983); **79**, 5105 (1983); **79**, 5119 (1983).
[10]M. S. Daw and M. I. Baskes, Phys. Rev. B **29**, 6443 (1984).
[11]H. Gollisch, Surf. Sci. **166**, 87 (1986).
[12]A. Sadiq, Phys. Rev. B **9**, 2299 (1974).
[13]M. Bowker and D. A. King, Surf. Sci. **71**, 583 (1978); **72**, 208 (1978).
[14]D. A. Reed and G. Ehrlich, Surf. Sci. **102**, 588 (1981); **105**, 603 (1981).
[15]G. E. Murch, Philos. Mag. A **43**, 871 (1981).
[16]M. Tringides and R. Gomer, Surf. Sci. **145**, 121 (1984).
[17]A. Sadiq and K. Binder, Surf. Sci. **128**, 350 (1983).
[18]W. Y. Ching, D. L. Huber, M. G. Lagally, and G.-C. Wang, Surf. Sci. **77**, 550 (1978).
[19]W. Kinzel, W. Selke, and K. Binder, Surf. Sci. **121**, 13 (1982).
[20]T.-M. Lu, G.-C. Wang, and M. G. Lagally, Phys. Rev. Lett. **39**, 411 (1977).
[21]P. Sahni and J. D. Gunton, Phys. Rev. Lett. **47**, 1754 (1981); P. Sahni, G. S. Grest, and S. A. Safran, *ibid.* **50**, 60 (1983).
[22]J. Salik, Phys. Rev. B **32**, 1824 (1985).
[23]E. V. Albano, J. M. Heras, P. Schrammen, M. Mann, and J. Holzl, Surf. Sci. **129**, 137 (1983).
[24]G. M. White and F. F. Abraham, J. Appl. Phys. **21**, 5348 (1970).
[25]E. S. Hood, B. H. Toby, and W. H. Weinberg, Phys. Rev. Lett. **55**, 2437 (1985).
[26]J. D. Doll, J. Chem. Phys. **73**, 2760 (1980); **74**, 1074 (1981).
[27]J. E. Adams and J. D. Doll, J. Chem. Phys. **74**, 1467 (1981).
[28]H. S. Johnston, *Gas Phase Reaction Rate Theory* (Ronald, New York, 1966), p. 48.
[29]A. F. Voter and J. D. Doll, J. Chem. Phys. **80**, 5832 (1984).
[30]N. Metropolis, A. Rosenbluth, M. N. Rosenbluth, A. Teller, and E. Teller, J. Chem. Phys. **21**, 1087 (1953).
[31]J. C. Keck, Discuss. Faraday Soc. **33**, 173 (1962); J. C. Keck, Adv. Chem. Phys. **13**, 85 (1967); C. H. Bennett, in *Diffusion*

in Solids: Recent Developments, edited by J. J. Burton and A. S. Nowick (Academic, New York, 1975); C. H. Bennett, in *Algorithms for Chemical Computation,* edited by R. E. Christofferson (American Chemical Society, Washington, D.C. 1977); R. L. Jaffe and J. B. Anderson, J. Chem. Phys. **54**, 2224 (1971); R. L. Jaffe, J. M. Henry, and J. B. Anderson, *ibid.* **59**, 1128 (1973); R. N. Porter, D. L. Thompson, L. M. Raff, and J. M. White, *ibid.* **62**, 2429 (1975); J. L. Skinner and P. G. Wolynes, *ibid.* **69**, 2143 (1978); **72**, 4913 (1980).

[32]D. Chandler, J. Chem. Phys. **68**, 2959 (1978); J. A. Montgomery, D. Chandler, and B. J. Berne, *ibid.* **70**, 4056 (1979); R. O. Rosenberg, B. J. Berne, and D. Chandler, Chem. Phys. Lett. **75**, 162 (1980).

[33]A. F. Voter and J. D. Doll, J. Chem. Phys. **82**, 80 (1985).

[34]A. F. Voter, J. Chem. Phys. **82**, 1890 (1985).

[35]A. Ossicini, R. Memeio, and F. Ciccacci, J. Vac. Sci. Technol. A **3**, 387 (1985).

[36]B. Mustaftschiev, J. Cryst. Growth **65**, 50 (1983).

[37]J. D. Weeks and G. H. Gilmer, Adv. Chem. Phys. **40**, 157 (1979).

[38]W. B. Phillips, E. A. Desloge, and J. G. Skofronick, J. Appl. Phys. **39**, 3210 (1968).

[39]K. Heinemann and H. Poppa, Thin Solid Films **33**, 237 (1976).

[40]A. Masson, J. J. Metois, and R. Kern, Surf. Sci. **27**, 463 (1971).

[41]D. W. Bassett, Surf. Sci **23**, 240 (1970).

[42]J. J. Metois, Surf. Sci. **36**, 269 (1973).

[43]P. Cowan and T. T. Tsong, Phys. Lett. **53A**, 383 (1975).

[44]H.-W. Fink and G. Ehrlich, Surf. Sci. **150**, 419 (1985).

[45]U. Landman and M. F. Shlesinger, Phys. Rev. B **16**, 3389 (1977).

[46]U. M. Titulaer and J. M. Deutch, J. Chem. Phys. **77**, 472 (1982).

[47]A. Milchev and I. Markov, Surf. Sci. **156**, 392 (1985).

[48]F. C. Frank and J. J. van der Merwe, Proc. R. Soc. London, Ser. A **198**, 205 (1949); **198**, 216 (1949).

[49]A. F. Voter (unpublished).

[50]A. F. Voter, J. Vac. Sci. Technol. A **4**, 1528 (1986).